19

Thermal Behavior of IGBT Module for EV (Electric Vehicle)

Mohamed Amine Fakhfakh, Moez Ayadi,
Ibrahim Ben Salah and Rafik Neji
University of Sfax/Sfax
Tunisia

1. Introduction

EVs are divided into three categories: the pure EV, the hybrid EV, and the fuel cell EV. Although these three types of electric vehicle have different system configuration, one (or more) motor drive system is always needed to convert electrical power into mechanical ones. Among the drive systems used for EV, induction motor system and permanent magnet motor systems are mostly used for their high power density, high efficiency.

The motor drive system for electric vehicle (EV) is composed of a battery, three phase inverter, a permanent magnet motor, and a sensor system. The inverter is a key unit important among these electrical components which converts the direct current of the battery into the alternating current to rotate the motor. Therefore, for predicting the dynamic power loss and junction temperature, the electro-thermal coupling simulation techniques to estimate the power loss and to calculate the junction temperature become important.

This paper describes a compact thermal model suitable for the electro-thermal coupling simulation of EV inverter module for two current control methods. We can predict the dynamic temperature rise of Si devices by simulating the inverter operation in accordance with the real EV running.

2. Dynamic model of the EV

As shown in Figure 1 and table 1, there are six forces acting on the electric vehicle: the rolling resistance force, the aerodynamic force, the aerodynamic lift force, the gravity force, the normal force, and the motor force.

2.1 Rolling resistance force

Rolling resistance is due the tires deforming when contacting the surface of a road and varies depending on the surface being driven on. It can be model using the following equation:

$$F_1 = f\, M_v\, g \tag{1}$$

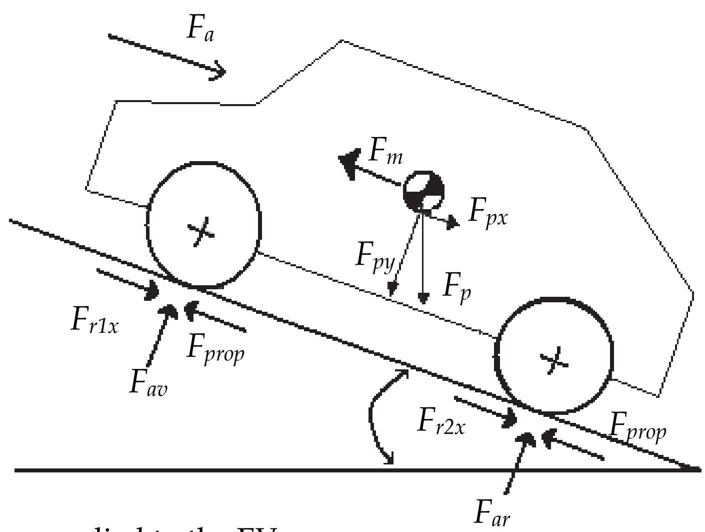

Fig. 1. Diagram of forces applied to the EV

F_{r1x}	Rolling resistance force
F_{r2x}	Rolling resistance force
F_{av}	Normal force
F_{ar}	Normal force
F_a	Aerodynamic force
F_{prop}	Thrust force
F_p	Gravity force
F_m	Motor force
θ	Slope angle with the horizontal

Table 1. Applied forces to EV

2.2 Aerodynamic force

Aerodynamic drag is caused by the momentum loss of air particles as they flow over the hood of the vehicle. The aerodynamic drag of a vehicle can be modeled using the following equation:

$$F_2 = \frac{1}{2}\rho S_f C_x V^2 \tag{2}$$

2.3 Gravity force

The gravity force can be calculated as follows:

$$F_3 = M_v g \sin\theta \tag{3}$$

2.4 Motor force

Using Newton's Second Law, we can deduce the motor force; it can be obtained by the following equation:

$$M_v \frac{dV}{dt} = \sum \vec{F}_{ext} = \vec{F}_m + \vec{F}_p + \vec{F}_a + \vec{F}_r \tag{4}$$

By projection on the (O, x) axis, we obtain:

$$F_m = M_v \frac{dV}{dt} + F_a + F_p + F_r \tag{5}$$

The power that the EV must develop at stabilized speed is expressed by the following equation:

$$P_{vehicle} = F_m V = (F_r + F_a + F_p + M_v \frac{dV}{dt})V \tag{6}$$

We deduce the expression of the total torque by multiplying equation (5) with the wheel radius R:

$$C_{vehicle} = C_r + C_a + C_p + M_v R \frac{dV}{dt} \tag{7}$$

Neglecting the mechanical losses in the gearbox, the t electromagnetic torque C_{em} developed by the motor is obtained by dividing the wheels torque $C_{vehicle}$ by the ratio reduction r_d.

$$C_{em} = \frac{1}{r_d}\left(C_r + C_a + C_p + M_v R \frac{dV}{dt}\right) \tag{8}$$

Figure 2 presents the dynamic model of the EV load, implemented under Matlab/simulink.

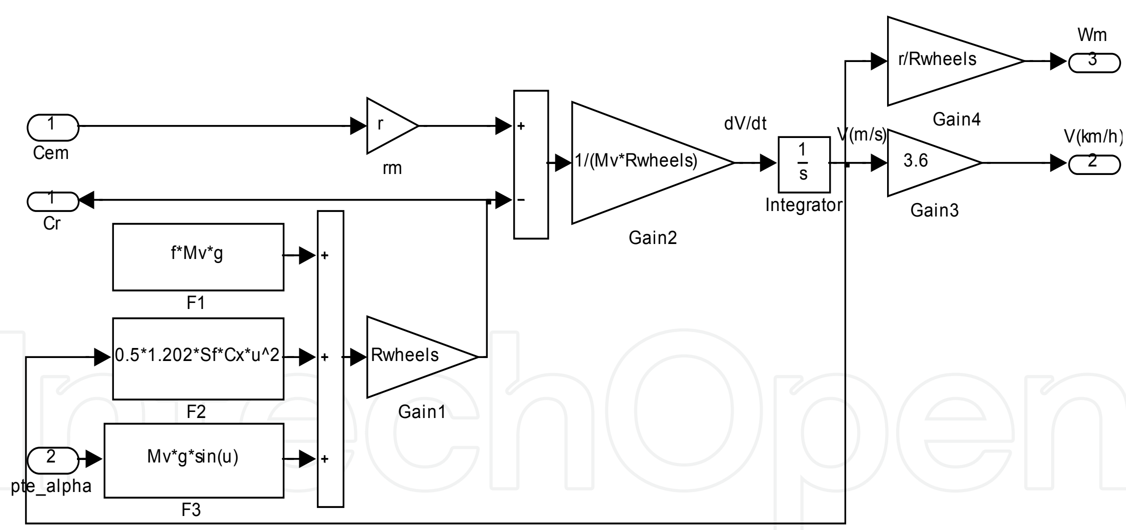

Fig. 2. SIMULINK dynamic model of electric vehicle

3. Electric motor control

Control of permanent magnet synchronous motor is performed using field oriented control. The stator windings of the motor are fed by an inverter that generates a variable frequency variable voltage. The frequency and phase of the output wave are controlled using a position sensor as shown in figure 3.

In our studie, we have used two types of current control, Hysteresis and PWM.

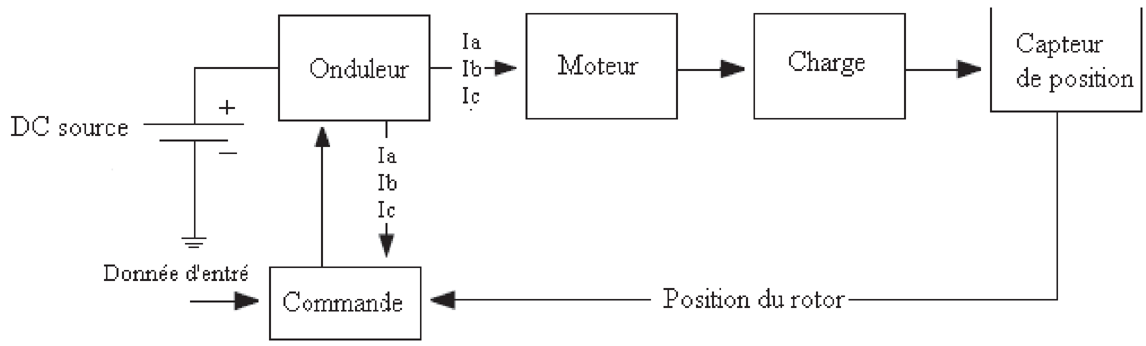

Fig. 3. Drive system schematic

3.1 PWM current controller

PWM current controllers are widely used. The switching frequency is usually kept constant. They are based in the principle of comparing a triangular carrier wave of desire switching frequency and is compared with error of the controlled signal [Bose, 1996].

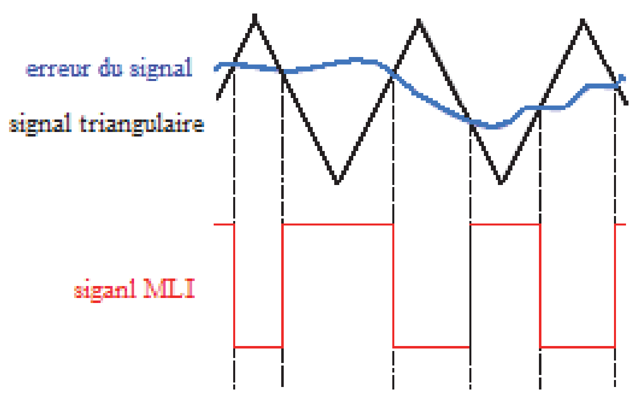

Fig. 4. PWM current controller

3.2 Hysteresis current controller

Hysteresis current controller can also be implemented to control the inverter currents. The controller will generate the reference currents with the inverter within a range which is fixed by the width of the band gap [Bose, 1996; Pillay et al., 1989].

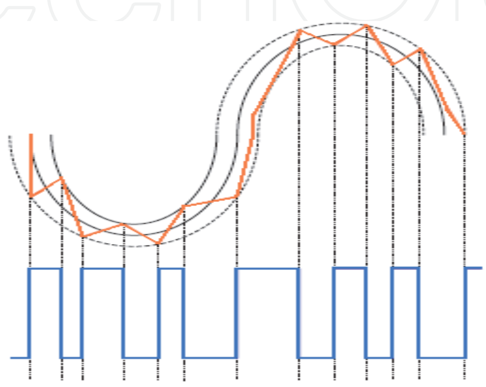

Fig. 5. Hysteresis current controller

4. Thermal model of IGBT module

The studied module is the Semikron module SKM 75GB 123D (75A/1200V) which contains two IGBTs and with two antiparallel diodes. The structure of the module contains primarily eight layers of different materials, each one of it is characterized by its thickness Li, its thermal conductivity Ki, density ρi and its heat capacity Cpi. Table 2 show the materials properties of the various layers of module as shown in figure 6. These values are given by the manufacturer and/or of the literatures [Dorkel et al., 1996; Uta et al., 2000; Thoams et al., 2000].

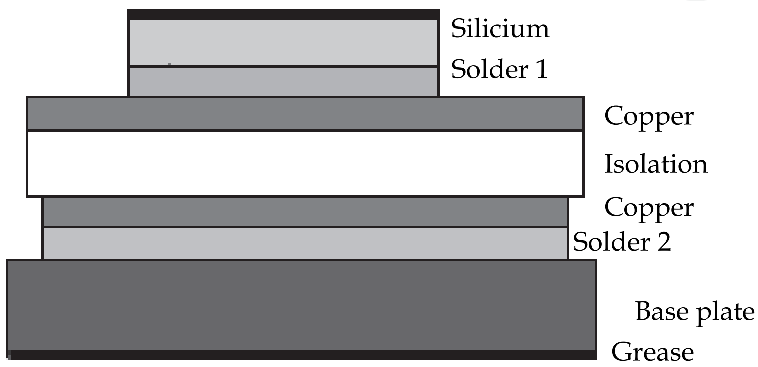

Fig. 6. Example of the module structure

Material	*L (mm)*	*K (W/mK)*	*ρCp (J/Kcm³)*
Silicium	0.4	140	1.7
Solder 1	0.053	35	1.3
Copper	0.35	360	3.5
Isolation	0.636	100	2.3
Copper	0.35	360	3.5
Solder 2	0.103	35	1.3
Base plate	3	280	3.6
Grease	0.1	1	2.1

Table 2. Thermal parameters of a power module

In the power module, the heating flow diffuses vertically and also laterally from the heating source. So, a thermal interaction happens inside the module between the adjacent devices when they operate together.

This thermal interaction depends from [Kojima et al., 2006; Ayadi et al., 2010; Fakhfakh et al., 2010]:

- The dissipated power value of the various components.
- The disposition of the chip components.
- The boundary condition at the heat spreader.

Figure 7 shows the thermal influence between the different components of the module. We notice that each component has a thermal interaction with the others and we supposed that each module have zero interaction with other modules.

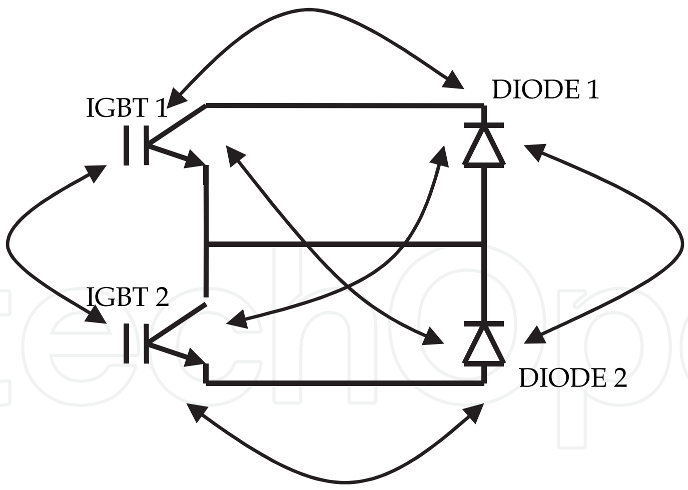

Fig. 7. Different thermal influences between the module components

Literature proposes some thermal circuit networks for electrothermal simulation for the semiconductor device. For example the finite difference method (FDM) and the finite element method (FEM). In our study we have used the FEM technique to model our inverter module. Figure 8 shows the thermal circuit example obtained by the FEM of IGBT1 without thermal interaction.

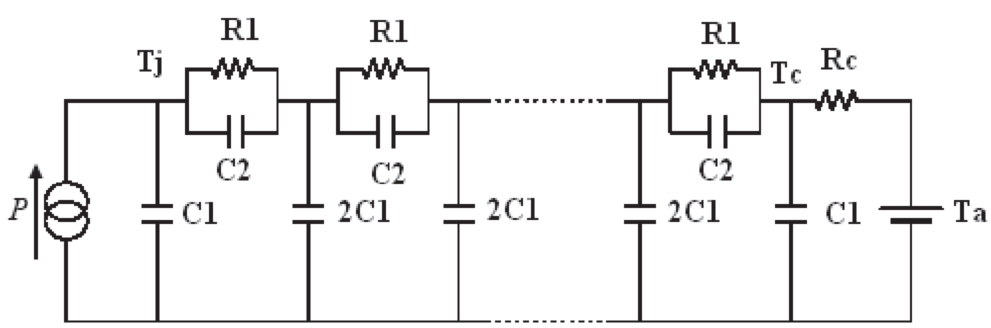

Fig. 8. Thermal circuit obtained by the FEM

Where:
- P is the input power dissipation device.
- Tj is the junction temperature.
- R1 is the thermal resistance.
- Rc is the convection resistance.
- C1 and C2 are thermal capacitance.
- Ta is the ambient temperature.

In order to introduce the thermal interaction between the different components of the module, we inserted three other current sources P1, P2 and P3. These sources are deduced from the structure of IGBT module [Drofenik et al., 2005; Hamada et al., 2006; Usui et al., 2006].

The source P1 is the power loss of DIODE1; it is introduced at the interface between the silicon and the copper materials because the IGBT1 and the DIODE1 ships are bounded on the same copper area. The source P2 and P3 are power loss of IGBT2 and DIODE2, they are introduced between solder 2 and base plate because all module components have the base plate as a common material. So the thermal circuit network of IGBT1 becomes as the figure 9.

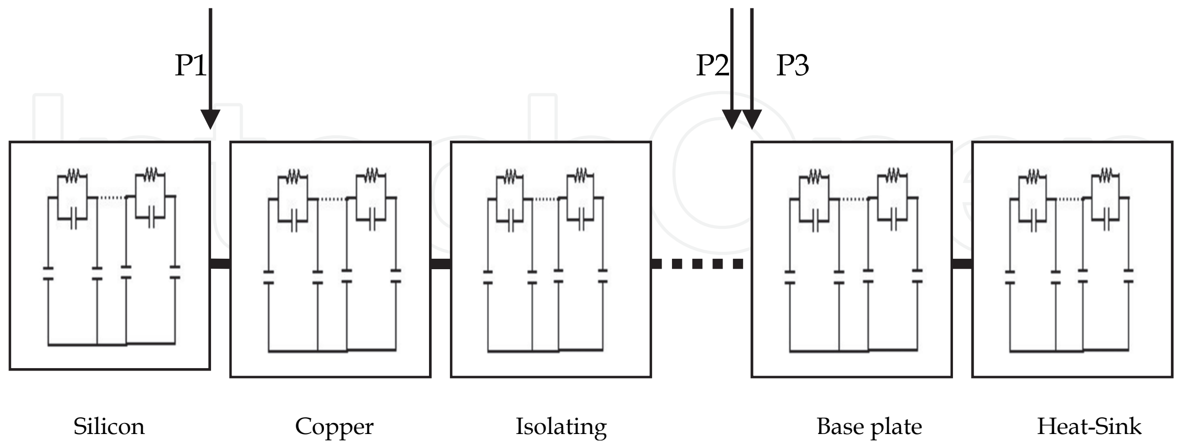

Fig. 9. Thermal model of IGBT module

5. Simulation and results

The PM motor drive simulation was built in several steps like abc phase transformation to dqo variables, calculation torque and speed, and control circuit [Ong, 1998; Roisse et al., 1998].
Parks transformation used for converting Iabc to Idq is shown in figure 10 and the reverse transformation for converting Idq to Iabc is shown in figure 11.

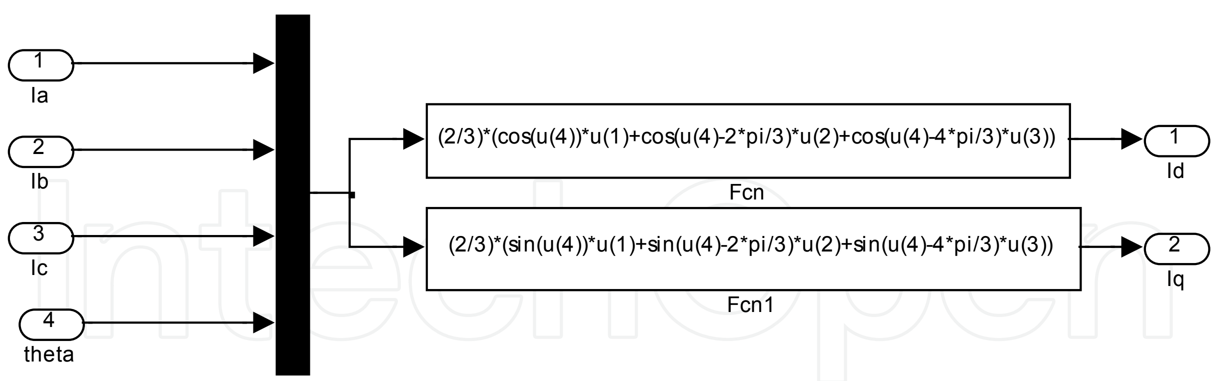

Fig. 10. Iabc to Idq bloc

The inverter is implemented in Simulink as shown in figure 12. The inverter consists of the "universal bridge" with the parameters of the IGBT module studied. All the voltages and the currents in the motor and the inverter can be deducted. The following figure shows the model of the inverter used.
For proper control of the inverter using the reference currents, current controllers are implemented generate the gate pulses for the IGBT's. Current controllers used are shown in figure 13 and 14.

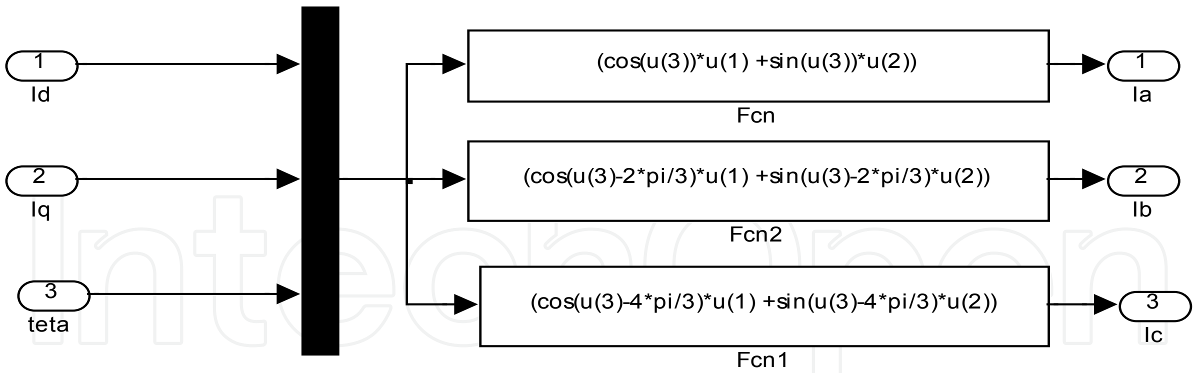

Fig. 11. Idq to Iabc bloc

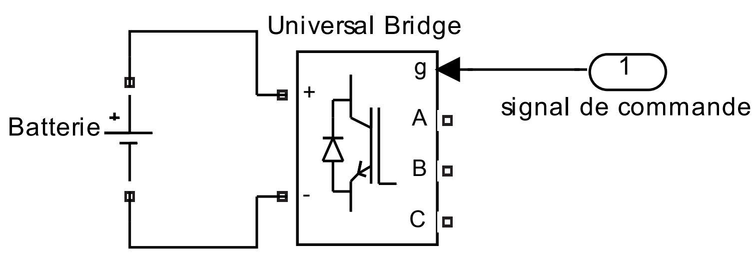

Fig. 12. Inverter model

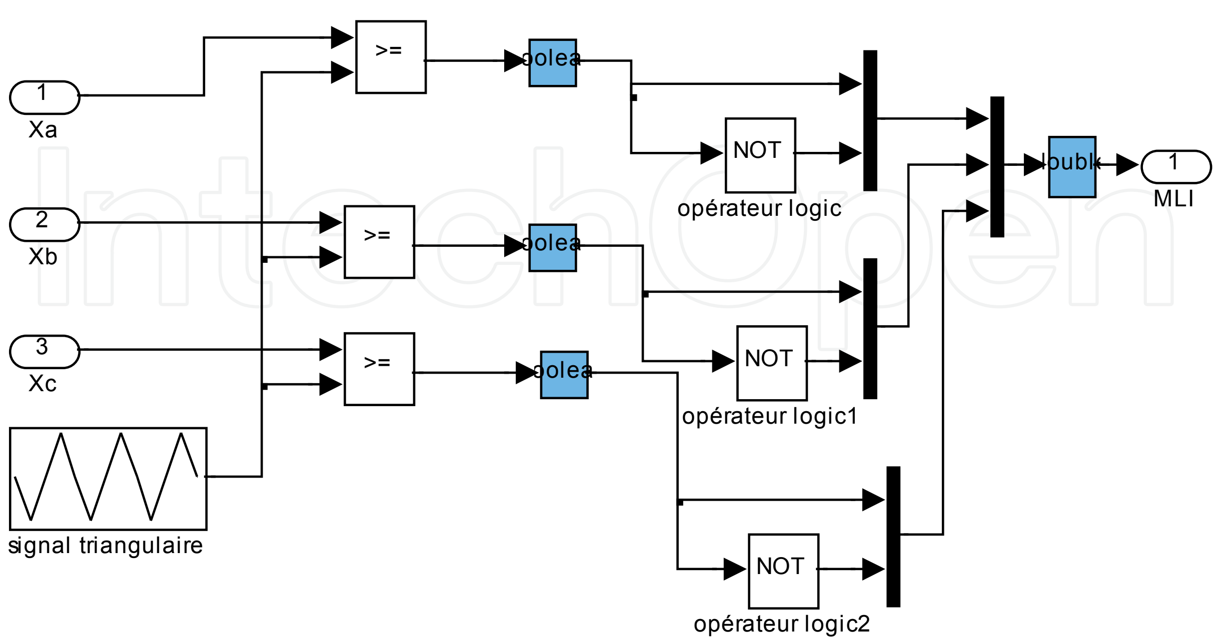

Fig. 13. PWM current controller

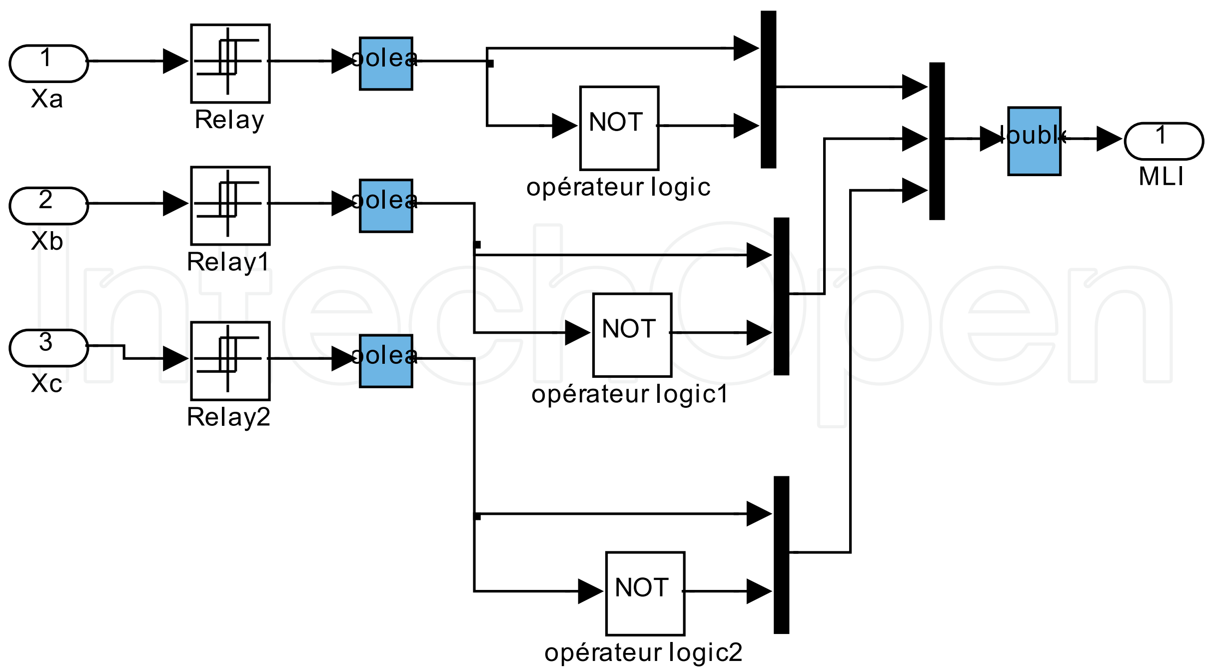

Fig. 14. Hysteresis controller

The complete system used for simulation and implemented in MATLAB / Simulink, is shown in Figure 15. This system was tested with two current controls, hysteresis and PWM control. The motor used is an axial flux Permanent Magnet Synchronous Motor (PMSM). For the simulation, we controlled the speed of EV at 30km / h.

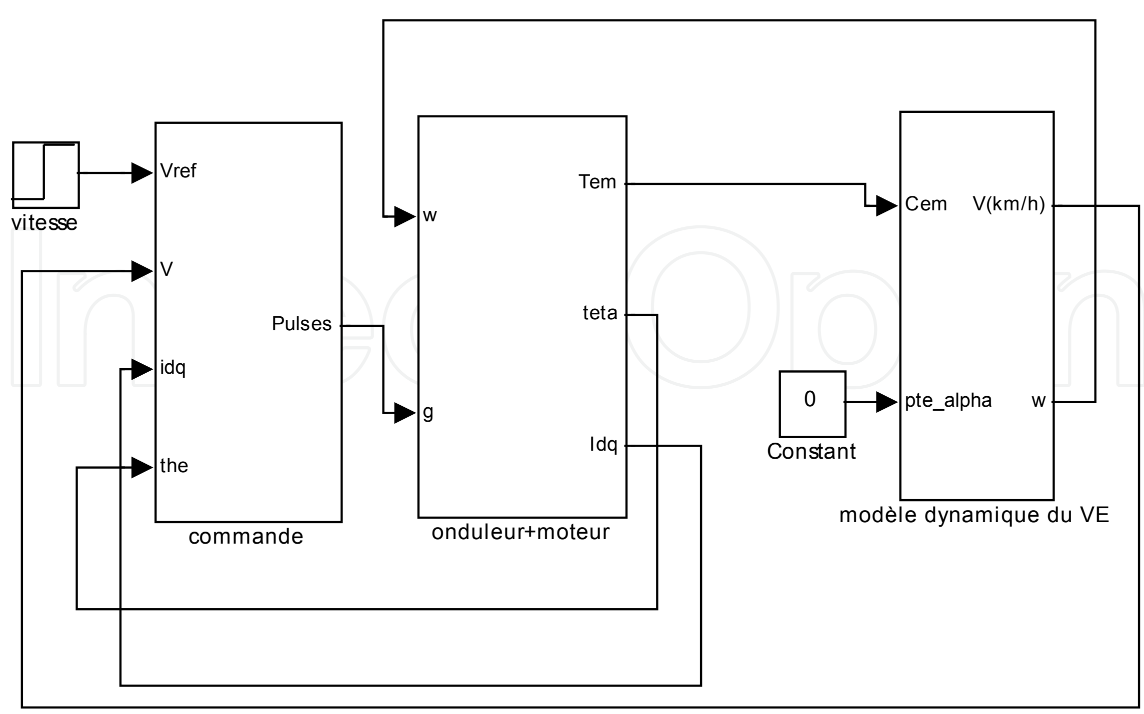

Fig. 15. PMSM in a traction chain

Figure 16 shows the EV speed regulated at 30km / h for the two types of control. We note that with the hysteresis control, we reach faster the steady state.

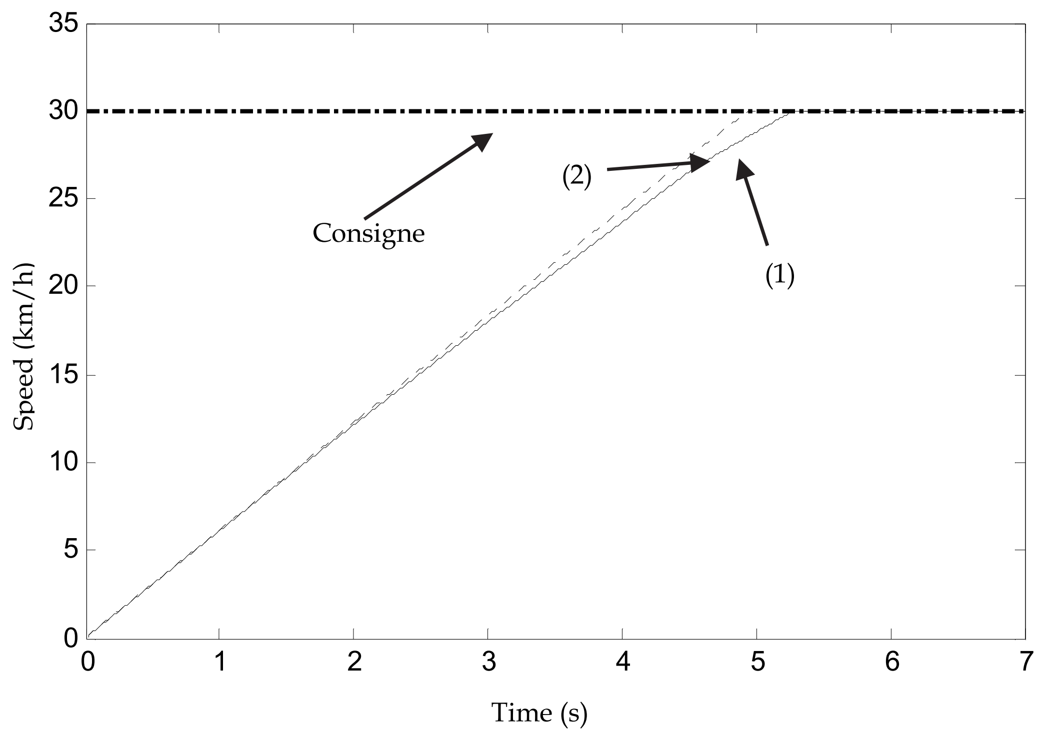

Fig. 16. EV speed; (1): with PWM controller; (2): with hysteresis controller

The stator phase currents corresponding to this regulation are represented by figure 17 and 18 Figure 19 and 20 show the IGBT1 and DIODE1 power losses for hysteresis and PWM current control respectively.

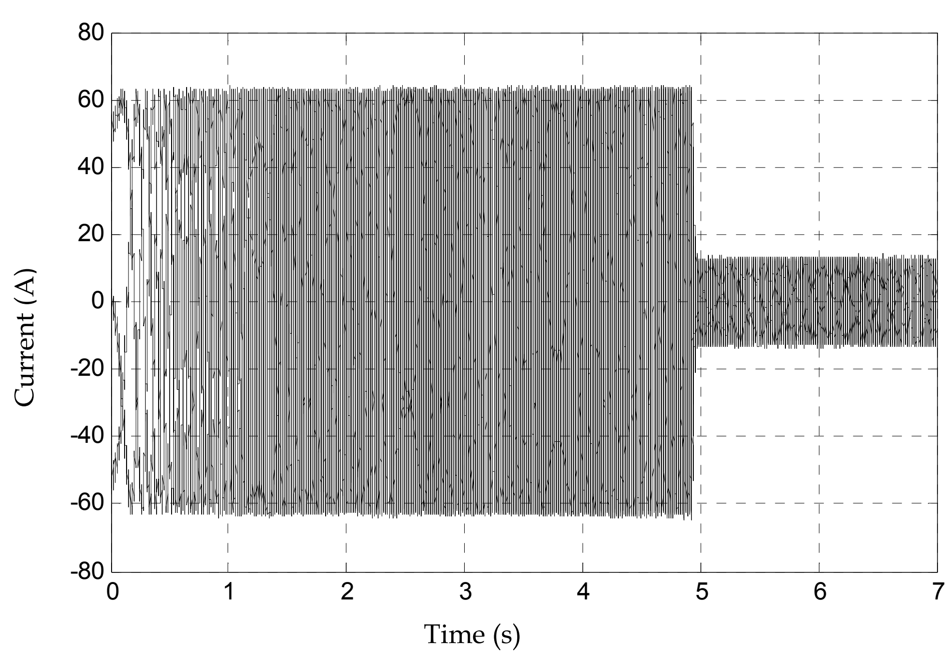

Fig. 17. Iabc currents with hysteresis control

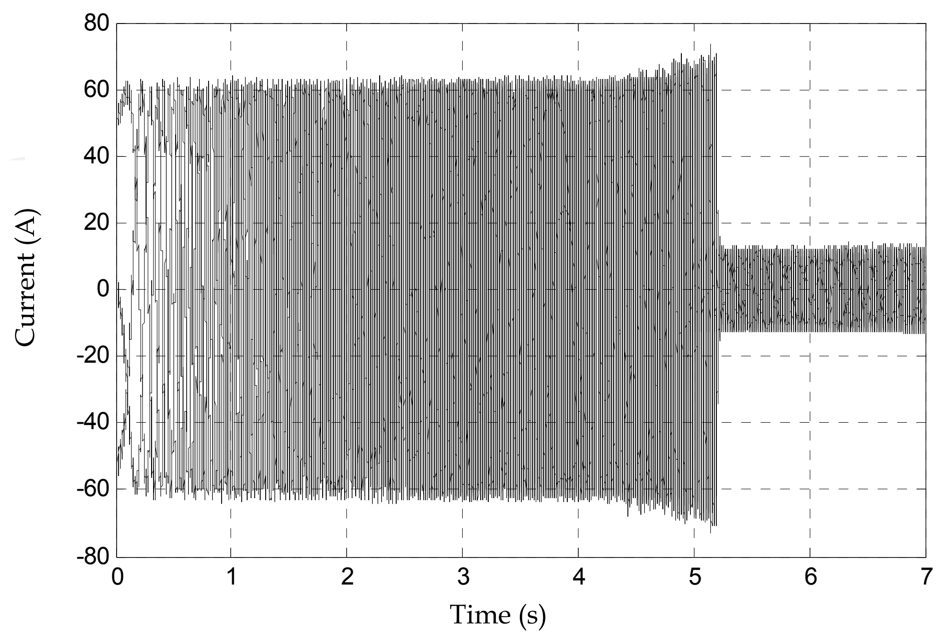

Fig. 18. Iabc currents with PWM control

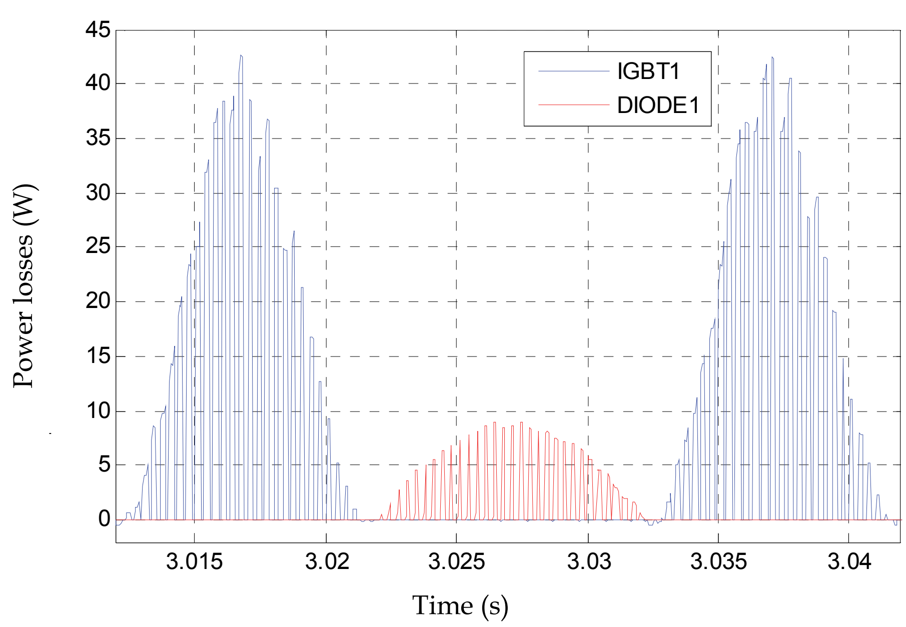

Fig. 19. IGBT1 and DIODE1 power losses with PWM control

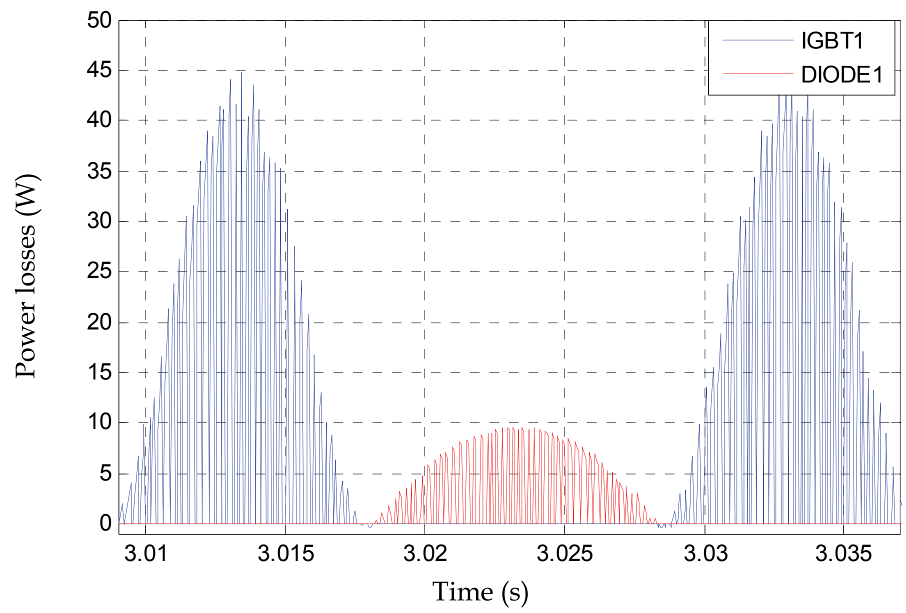

Fig. 20. IGBT1 and DIODE1 power losses with hysteresis control

Figure 21 and 22 show the IGBT1and DIODE1 junction temperature obtained by the two types of current control. It is very clear that the junction temperature of IGBT1 and DIODE1 is higher for the hysteresis control; this is due by the increase of power dissipation of the module components this type of control.

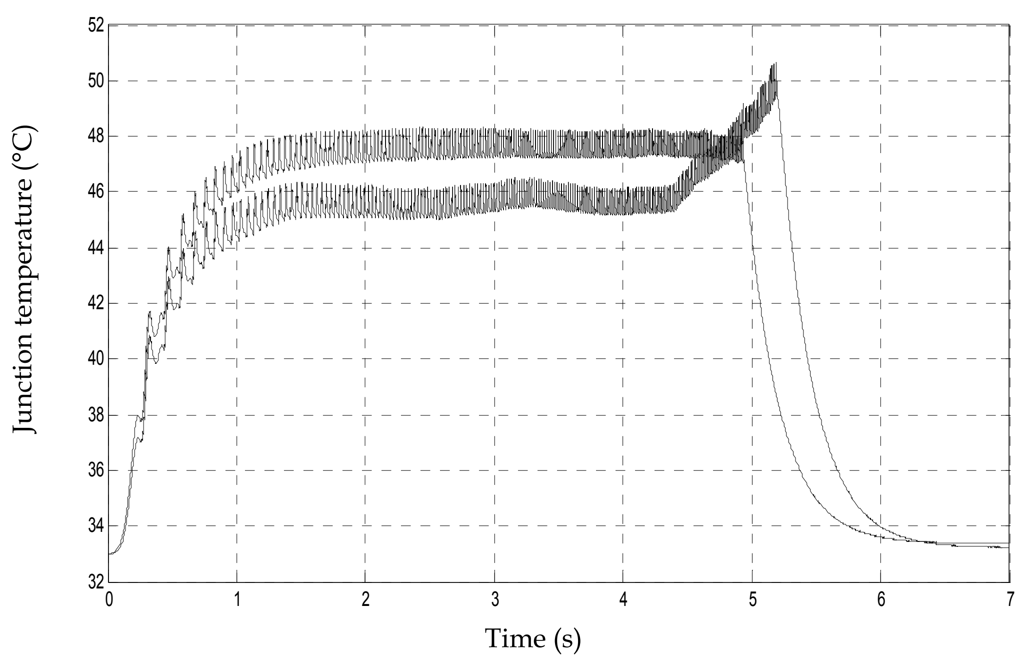

Fig. 21. IGBT1 junction temperature

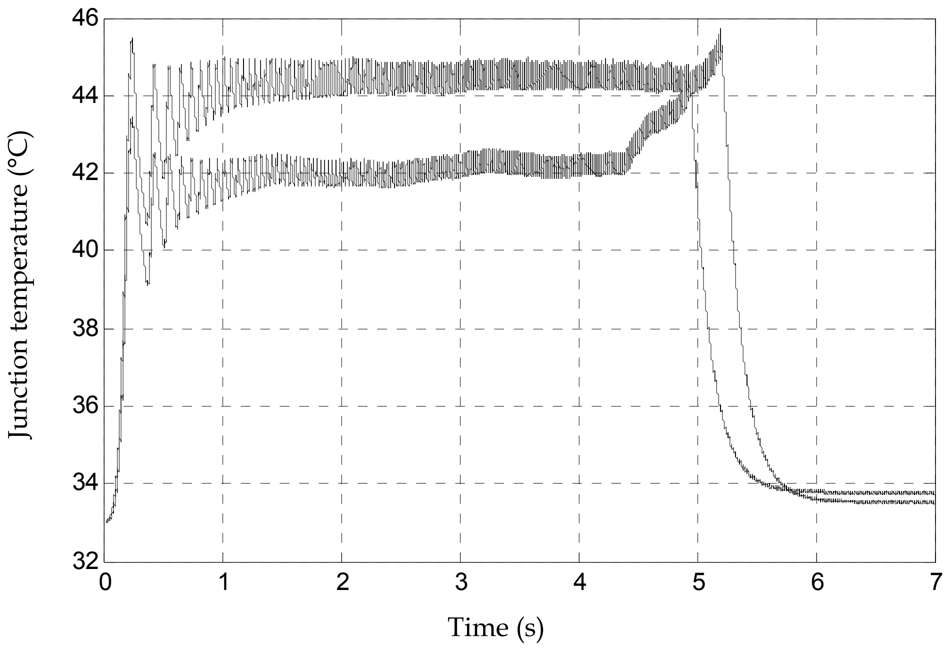

Fig. 22. DIODE1 junction temperature

6. Conclusion

A detailed dynamic model for EV was studied using two current control systems. MATLAB / Simulink were chosen from several simulation tools because of its flexibility in working with analog and digital devices, it is able to represent real-time results with the simulation time reduced. A comparative study was carried out in terms of switching frequency for power dissipated by the components of the inverter and junction temperature. The hysteresis current control has a variable switching frequency that depends on the hysteresis band, this type of control allows for fast simulations with a shorter time. The PWM current control has a fixed frequency switching and allows having junction temperatures lower than the hysteresis control.

7. References

B. K. Bose, Power Electronics and Variable Frequency Drives. (1996). 1 ed: Wiley, John & Sons

P. Pillay & R. Krishnan. (1989). Modeling, simulation, and analysis of permanent-magnet motor drives. I. The permanent-magnet synchronous motor drive. *Industry Applications, IEEE Transactions on*, vol. 25, pp. 265-273

Jean-Marie Dorkel, Patrick Tounsi, & Philippe Leturcq. (1996). Three-Dimensional thermal Modeling Based on the Two-Port Network Theory for Hybrid or Monolithic Integrated Power Circuits. IEEE Transaction on Electronics Devices, vol. 19, NO. 4, pp. 501-507

Uta Hecht & Uwe Scheuermann. (2000). Static and Transient Thermal Resistance of Advanced Power Modules. *Semikron Elektronik GmbH*, Sigmundstr. 200, 90431 Nürnberg (Germany).

Thomas Stockmeier. (2000). Power semiconductor packaging-a problem or a resource? From the state of the art to future trends. *Semikron Elektronik GmbH*, Sigmundstr. 2000, 90431 Nürnberg (Germany)

M. Ayadi, M.A. Fakhfakh, M. Ghariani, & R. Neji. (2010). Electrothermal modeling of hybrid power modules. *Emerald, Microelectronics International (MI),* volume 27, issue 3, 2010, pp. 170-177

M.A. Fakhfakh, M. Ayadi, and R. Neji. Thermal behavior of a three phase inverter for EV (Electric Vehicle). *in Proc of 15th IEEE Mediterranean Electromechanical Conference (MELECON'10)*, Valletta, Malta, April 25-28, 2010, C4P-E24-3465, pp.1494-1498.

Kojima, et al. Novel Electro-thermal Coupling Simulation Technique for Dynamic Analysis of HV (Hybrid Vehicle) Inverter. *Proceedings of PESCO6*, pp. 2048-2052, 2006.

Hamada. Novel Electro-Thermal Coupling Simulation Technique for Dynamic Analysis of HV (Hybrid Vehicle) Inverter," Proc. of 7thIEEE Power Electronics Specialists Conference (PESC 2006), pp.2048-2052, 2006

U. Drofenik & J. Kolar. (2005). A Thermal Model of a Forced-Cooled Heat Sink for Transient Temperature Calculations Employing a Circuit Simulator. *Proceedings of IPECNiigata* 2005, pp. 1169-1177, 2005

M. Usui, M. Ishiko, "Simple Approach of Heat Dissipation Design for Inverter Module," Proc. of International Power Electronics Conference (IPEC 2005), pp. 1598-1603, 2005.

C. M. Ong. (1998). Dynamic simulation of electric machinery using MATLAB/Simulink.

H. Roisse, M. Hecquet, P. Brochet. (1998). Simulation of synchronous machines using a electric-magnetic coupled network model. IEEE Trans. on Magneticss, vol.34, pp.3656-3659, 1998.

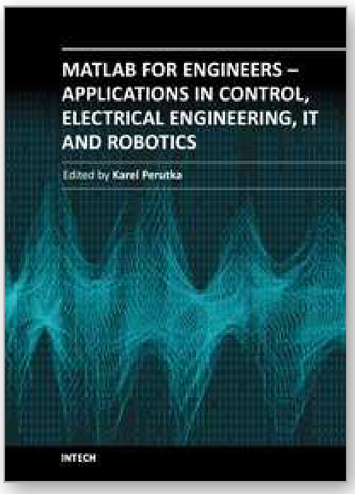

MATLAB for Engineers - Applications in Control, Electrical Engineering, IT and Robotics
Edited by Dr. Karel Perutka

ISBN 978-953-307-914-1
Hard cover, 512 pages
Publisher InTech
Published online 13, October, 2011
Published in print edition October, 2011